The International Journal of Advanced Manufacturing Technology (2024) 130:2587–2600
https://doi.org/10.1007/s00170-023-12755-6

ORIGINAL ARTICLE

Effect of aerostatic spindle dynamic characteristics on the medium frequency waviness error of silicon wafer surface

Meng Li[1] · Xianglong Zhu[1] · Renke Kang[1] · Jiasheng Li[1] · Jiahui Xu[1]

Received: 11 September 2023 / Accepted: 24 November 2023 / Published online: 19 December 2023
© The Author(s), under exclusive licence to Springer-Verlag London Ltd., part of Springer Nature 2023

Abstract
In the process of ultra-precision grinding, the dynamic characteristics of the aerostatic spindle system are important factors affecting the machined surface morphology. In order to study the influence of the dynamic characteristics of the spindle system on the medium frequency waviness error of the silicon wafer surface, this paper first establishes a dynamic model of the aerostatic spindle system considering the grinding force and the eccentricity of the spindle rotor based on Newton's law and the angular momentum law, analyzes the dynamic response and frequency characteristics of the spindle system, and conducts modal tests on the spindle system to verify the accuracy of the dynamic model. Then, the power spectral density analysis of the surface morphology of the silicon wafer after grinding is carried out, and the frequency components of the intermediate frequency band of the silicon wafer surface are obtained. Compared with the characteristic frequency of the spindle system and the vibration displacement curve of the end, it is found that the dynamic characteristics of the aerostatic spindle system are the main reason for the medium frequency waviness error on the surface of the silicon wafer. Finally, an optimization scheme for structural improvement of the aerostatic spindle system is given. Through the finite element analysis of the grinding machine, it is found that the vibration displacement of the spindle end after optimization is reduced by 52.8 % compared with that before optimization, which shows that the optimization scheme is effective and provides a reference for the structural design of the aerostatic spindle system.

Keywords Aerostatic spindle system · Dynamic response · Medium frequency waviness error · Finite element analysis

1 Introduction

Ultra-precision grinding of silicon wafers is mainly used for wafer flattening during wafer preparation and backside thinning in the IC back-end process. With the continuous increase of IC integration, the surface of silicon wafer after grinding needs to have high precision and high surface and subsurface integrity [1]. This puts forward higher requirements for the dynamic characteristics and motion characteristics of the grinding machine structure, so how to further improve the surface accuracy of the silicon wafer after grinding has become an important issue in ultra-precision grinding.

✉ Xianglong Zhu
zhuxianglong@dlut.edu.cn

[1] State Key Laboratory of High-Performance Precision Manufacturing, Dalian University of Technology, Dalian 116024, People's Republic of China

There are generally three surface errors on the surface of the workpiece after ultra-precision grinding, namely shape error, surface intermediate frequency waviness error, and surface roughness error [2]. The shape error is caused by the error of the grinding machine in the operation process, which belongs to the low frequency error. This can be eliminated by optimizing the feed system of the machine tool and improving the running accuracy of the machine tool. The surface roughness error is a high-frequency error, mainly caused by the size of the grinding wheel, the physical properties of the grinding material and the selection of grinding parameters, and the surface roughness of the machined surface can be reduced by selecting different grinding parameters. The medium frequency waviness error of the grinding surface is the intermediate frequency error between low frequency and high frequency, which is caused by the mutual vibration between the diamond grinding wheel and the silicon wafer during the grinding process. The vibration of the grinding wheel and the workpiece is mainly due to the vibration of the main shaft system, the fluctuation of the

air source pressure, the fluctuation of the cutting force, the vibration of the machine tool structure and the vibration of the foundation, and the final performance is the error of the workpiece surface topography. The vibration between the grinding wheel and the workpiece is the link between the dynamic performance of the grinder and the surface topography of the workpiece. In order to further improve the accuracy of silicon wafer grinding processing, many scholars have done a lot of research in recent years.

Tao et al. [3] of Tsinghua University conducted a dynamic modeling of the grinding wheel spindle and explored the influence of different grinding parameters and vibration frequencies on the surface ripple characteristics. Yang et al. [4] established the dynamic finite element analysis of the air spindle, fitted the vibration trajectory of the tool during the cutting process, and improved the amplitude of the surface fringes by optimizing the design of the spindle. Guo et al. [5] proposed a frequency-domain dynamic response method to optimize the dynamic performance of the spindle system of the grinding machine from the perspective of spindle imbalance and frequency response function. Wu et al. [6] studied the influence of spindle drift error on the machined surface. A mechanical model of the spindle system considering mass eccentricity was established. Gao et al. [7] established a dynamic model of machine tools considering the fluid-structure interaction effect and studied the intrinsic relationship between the machining surface and the dynamic performance of the machine tool. Chen et al. [8] established a transient computational fluid dynamics (CFD) analysis simulation model to study the dynamic characteristics of aerostatic spindles under unstable conditions. Dong et al. [9] popularized the dynamic model of spindle vibration and studied the influence of spindle vibration on surface morphology under different cutting forces. Chen et al. [10] propose a new model to analyze the relationship between axle vibration to surface roughness (SR) and subsurface damage (SSD) depth. Liu et al. [11] uses the computational fluid dynamics (CFD) method to give the aerodynamic forces on the slide and under the shank when the tool is machining different areas. Meng et al. [12] proposed a microstructured grinding wheel precision grinding kinetic modeling and discussed the influence of grinding wheel topography on the amplitude and frequency of grinding force. Niu et al. [13] studied the combined effects of cutting data, tool geometry, and runout on regenerative flutter behavior. Yin et al. [14] proposed a modal decoupling method based on running deflection shape (ODS) and structural sensitivity analysis to identify structural vibrations on surface topography during manufacturing. Wei et al. [15] established a high-precision spindle system model and found that the intermediate frequency waveform of the machined surface matched the vibration waveform. An et al. [16] proposed a method for measuring the motion error of the aerostatic pressure spindle online using the nanoscale and discussed the main sources of the ripple error of the crystal processing surface. Ding et al. [17] used the finite element method to establish the dynamic model of the rotating parts and proved that the deformation of the flying tool head and the tool holder has a great influence on the displacement of the tool tip.

In addition, many scholars have also done a lot of research on the simulation of the morphology of the processed surface and how the process parameters affect the processed surface. Yao et al. [18] proposed a method to improve the flatness of the grinding wafer by changing the process parameters and changing the inclination angle of the grinding wheel shaft. Chen et al. [19] established a surface topography model of the coupling effect of spindle turning dynamics and analyzed the effects of spindle speed, cutting width, and feed rate on surface morphology. Tao et al. [20] considered the random distribution of the position and size of the grinding wheel grain, reshaped the grinding wheel morphology, and established a simulation model of the wafer surface morphology. Sun et al. [21] discusses the influence of grinding wheel grinding parameters on surface height by coupling the results of the grinding system dynamics analysis into the particle trajectory equation. Zhu et al. [22] studied the material removal mechanism of TiC/Ni cermet through nanoindentation analysis and diamond scratch test and analyzed and explored the surface damage mechanism caused by grinding. Li et al. [23] has conducted theoretical and experimental research on the generation of surface morphology in freeform STS machining. Yin et al. [24] established a surface wavy formation model, and the experimental results show that this study can help optimize grinding conditions to improve surface quality and tribological properties. Zhang et al. [25] established a new contact stiffness model for the rough surface of different processing stripes and analyzed the influence of different conditions on the contact stiffness of the striped surface.

In summary, most of the current researchers basically only model and analyze the dynamic performance of silicon wafer grinding surfaces or silicon wafer grinding machines alone, and do not establish a connection between the two. In this paper, the wafer ultra-precision grinding machine model GP300 is taken as the research object. The dynamic model of the aerostatic spindle system of the grinding machine is established, and the dynamic response of the spindle system is analyzed. The dynamic response characteristics of the spindle system are compared and analyzed with the characteristic frequencies of the intermediate frequency band on the surface of the silicon wafer after grinding, and it is verified that the intermediate frequency waviness error of the surface of the silicon wafer is caused by the dynamic characteristics of the aerostatic pressure spindle system of the grinding machine.

2 Study of aerostatic spindle system dynamics

In this section, the theoretical modeling method is used to analyze the dynamic modeling of the aerostatic spindle system. Firstly, the dynamic equation of the axle system in the error sensitive direction (Z direction) is established by using Newton's second law and angular momentum law. Then, the second-order Runge-Kuta method is used to solve and analyze the model equation, and finally the dynamic characteristics of the aerostatic spindle system in the error-sensitive direction are obtained.

2.1 Aerostatic spindle system dynamics modeling

Wafer ultra-precision grinding machine is mainly composed of air static pressure spindle, grinding wheel adapter plate, cup diamond grinding wheel, granite bed, column, etc. The grinder has sufficient stiffness and good vibration resistance. Among them, the aerostatic spindle, the grinding wheel adapter plate and the cup diamond grinding wheel constitute a grinding system, and its dynamic characteristics have an important influence on the surface quality and morphology of the silicon wafer. Figure 1 is the structure of the wafer ultra-precision grinding machine and the grinding principle of silicon wafer. In the grinding process, the silicon wafer is first adsorbed on the vacuum sucker by vacuum. The cup-shaped diamond grinding wheel is connected to the aerostatic spindle through the grinding wheel adapter plate. The workpiece spindle and the grinding wheel rotate around their respective rotation axes, and the grinding wheel moves continuously along the axis.

In order to study the dynamic characteristics of the grinding machine aerostatic spindle system in the grinding error sensitive direction. The grinding wheel, the grinding wheel adapter, and the aerostatic spindle are simplified into a multi-spring-mass-damping system, as shown in Fig. 2. Among them, since the spindle rotor is supported by an aerostatic bearing, the stiffness of the spindle rotor is much higher than the stiffness of the air film in the air bearing. Therefore, the rotor can be regarded as a single point mass

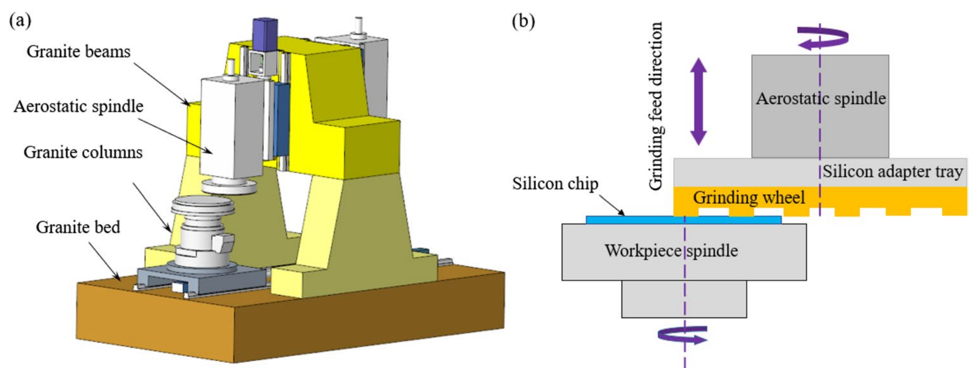

Fig. 1 Ultra-precision wafer grinding. **a** Wafer grinding machine structure diagram. **b** Principle of wafer grinding

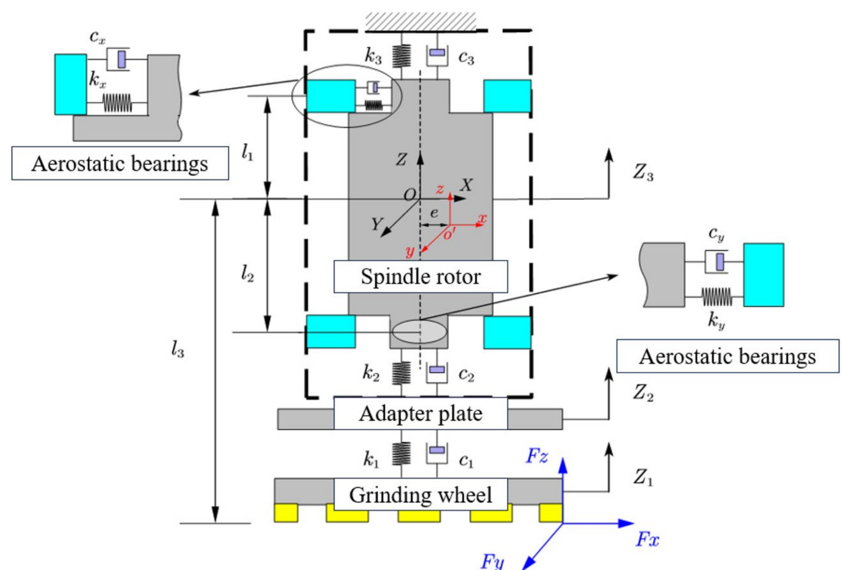

Fig. 2 Equivalent dynamic model of an aerostatic spindle system

with a certain eccentricity, and the aerostatic bearing can be regarded as a spring damper with constant stiffness and damping placed along the X and Y directions. In addition, the grinding wheel and the adapter plate, the adapter plate and the spindle rotor are all connected by bolts, so the joint surface of the three can be equivalent to a spring damper that extends the axial direction.

In the actual grinding process, due to the uneven quality of the spindle rotor, the center of mass of the rotor is not fixed on the ideal rotation center line of the spindle. Moreover, there are some factors such as grinding force during grinding, so the grinding wheel will have translational motion in the three directions of X, Y, and Z and tilt motion in the three directions during the rotation process. However, because the grinding wheel is grinding in the Z direction, the vibration of the grinding wheel during the rotation process only affects the translational motion in the Z direction and the tilt motion around the X axis and the Y axis, as shown in Fig. 3.

For the Z-direction translational vibration motion of the grinding wheel in the actual grinding process. The Z-direction force analysis of the grinding wheel, the adapter plate and the spindle rotor is carried out separately, as shown in Fig. 4. According to Newton's second law, the acceleration of the translational motion of an object is related to the force it is subjected to:

$$\vec{F} = m\vec{a} \tag{1}$$

Therefore, according to the model of grinding force established by Zhu's work [26] and the force of each component of the spindle system, the dynamic equation of the Z direction of the spindle system is established, as shown in Eq. (2).

$$\begin{cases} m_1\ddot{z}_1 + c_1(\dot{z}_1 - \dot{z}_2) + k_1(z_1 - z_2) = F_z \\ m_2\ddot{z}_2 + c2(\dot{z}_2 - \dot{z}_3) + k_2(z_2 - z_3) - k_1(z_1 - z_2) - c1(\dot{z}_1 - \dot{z}_2) = 0 \\ m3\ddot{z}_3 + c_3\dot{z}_3 + k_3z_3 - k_2(z_2 - z_3) - c_2(\dot{z}_2 - \dot{z}_3) = 0 \end{cases} \tag{2}$$

In addition, in order to derive the vibration displacement equation of the tilt motion of the spindle system in the error sensitive direction. Firstly, an inertial coordinate system O

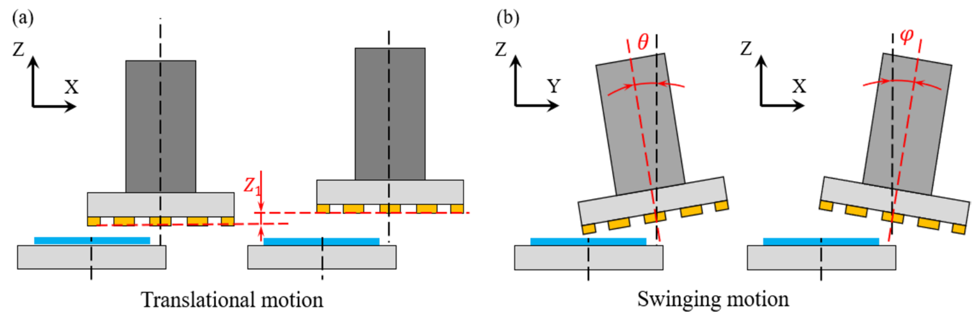

Fig. 3 Vibration form of spindle system. **a** The grinding wheel spindle is translated in the Z direction. **b** The rotation of the grinding wheel spindle around the X and Y axes

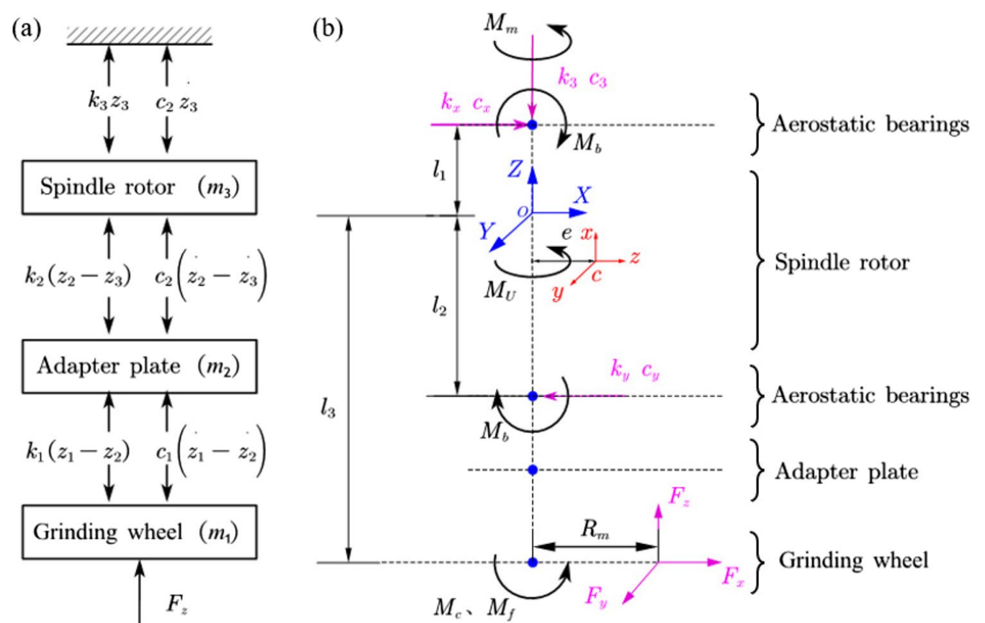

Fig. 4 Force analysis of aerostatic spindle system. **a** Translational motion analysis of spindle systems. **b** Spindle system tilt motion analysis

(xyz) is defined on the ideal geometric center of the spindle rotor. Since the grinding wheel spindle rotor is regarded as a single point mass with a certain eccentricity, the center of mass of the rotor is not fixed on the ideal coordinate system in the process of grinding rotation. Therefore, a fixed coordinate system *C (xyz)* is defined on the center of mass of the rotor, as shown in Fig. 5. The stationary coordinate system *C (xyz)* is obtained by the translational motion and tilt motion of the inertial coordinate system *O (xyz)*.

Equation (3) is the equation derived from the Euler angle to obtain the transformation of the fixed coordinate system *C (xyz)* with the three axes of the inertial coordinate system *O (xyz)* [3]. where θ, ∅, and Ω are the rotation angles around the three coordinate axes of X, Y, and Z, where $\Omega = \omega t$, ω represents the angular velocity of the grinding wheel spindle rotor, and t represents the time of rotation.

$$\begin{bmatrix} c_x \\ c_y \\ c_z \end{bmatrix} = \begin{bmatrix} \cos\Omega & \sin\Omega & \theta\sin\Omega - \Phi\cos\Omega \\ -\sin\Omega & \cos\Omega & \theta \\ \phi & -\theta & 1 \end{bmatrix} \begin{bmatrix} O_x \\ O_y \\ O_z \end{bmatrix} \tag{3}$$

Since the grinding wheel spindle is a symmetrical structure. Therefore, the inertia tensor of the grinding wheel spindle rotor in the stator coordinate system can be expressed as shown in Eq. 4 [27], where J_x, J_y, and J_z respectively represent the moment of inertia of the fixed body coordinate system *C (xyz)* around the X, Y, and Z axes in the ideal coordinate system *O (xyz)*, e represents the distance of the spindle rotor mass extension radial eccentricity, l_1 and l_2 represent the distance of the ideal geometric center from the bearings at both ends of the aerostatic spindle, and m represents the mass of the spindle rotor.

$$J = \begin{bmatrix} J_x & 0 & -me(l_1 - l_2) \\ 0 & J_y & -me(l_1 - l_2) \\ -me(l_1 - l_2) & -me(l_1 - l_2) & J_z \end{bmatrix} \tag{4}$$

In the actual grinding process, the grinding wheel spindle system will be subjected to the external torque caused by the external force. Among them, the servo motor will generate the driving torque M_m around the Z axis. The cutting forces along the Y and Z axes at the end of the grinding wheel will create a cutting moment around the X direction of the spindle system, and the cutting forces along the X axis will create a cutting moment in the Y and Z directions of the system. In addition, due to the existence of friction, there will also be friction torque M_f inside the system, as shown in Eq. (5), where d ($i = x, y, z$) is the air viscous Angle damping. Finally, the static bearing will also produce external torque M_b on the main shaft rotor in the X and Y directions, and the numerical value is the product of the deflection angle of the main shaft rotor and the bearing force on the rotor [24].

$$\begin{aligned} M_\mathrm{m} &= [0\ \ 0\ \ M]^T \\ M_c &= R\left[F_y l_3 + F_z R_w\ \ F_x l_3\ \ F_x R_w\right]^T \\ M_f &= \left[d_x\dot{\theta}\ \ d_y\dot{\phi}\ \ d_z\omega\right]^T \\ M_b &= \begin{bmatrix} \left[(k_x + k_y)(l_1^2 + l_2^2) + k_z R_m^2\right]\theta \\ \left[(k_x + k_y)(l_1^2 + l_2^2) + k_z R_m^2\right]\phi \\ 0 \end{bmatrix} \end{aligned} \tag{5}$$

In addition, because the grinding wheel rotor is regarded as a single point mass with eccentricity, the dynamic unbalance force caused by the asymmetry of mass distribution will also occur during the rotation process. The dynamic unbalance force increases linearly with the square of unbalance and rotational speed, as shown in Eq. (6). Among them, m represents the mass of the spindle rotor, e represents the eccentricity of the rotor, U is the unbalance of the rotor, F_u represents the dynamic unbalance force, ω is the angular velocity of the spindle rotation, and M_U is the dynamic unbalance moment caused by the uneven mass distribution of the spindle.

$$\begin{aligned} U &= m \times e \\ F_u &= U \times \omega^2 \\ MU &= \left[0\ \ 0\ \ F_u e\right] \end{aligned} \tag{6}$$

Combining the above factors, according to the law of angular momentum, the angle of rotation of the grinding wheel spindle system around the X and Y axes can be expressed as [24]:

$$J \cdot \omega_c + \omega_c \times (J \cdot \omega_c) = M_m + Mc + M_f + M_b + M_U \tag{7}$$

Finally, the combined Eqs. (2) and (7) can be further derived from the translational motion equation of the

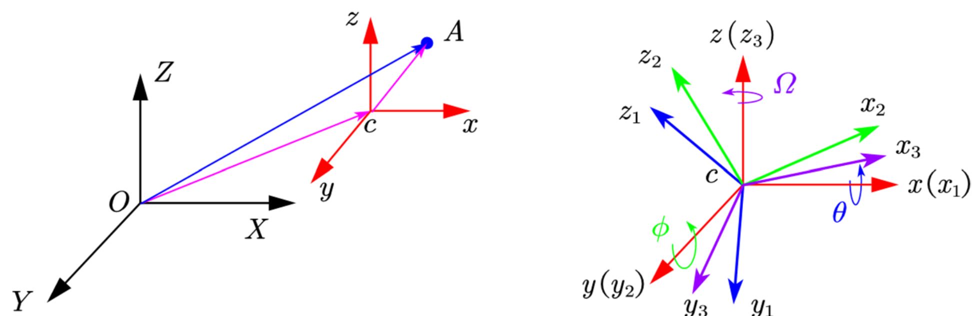

Fig. 5 The form of motion of a fixed coordinate system relative to an inertial coordinate system

grinding wheel spindle system in the sensitive direction and the tilting motion equation around the X and Y axes, as shown in Eq. (8):

$$\begin{cases} m_1\ddot{z}_1 + c_1\left(\dot{z}_1 - \dot{z}_2\right) + k_1\left(z_1 - z_2\right) = F_z \\ m_2\ddot{z}_2 + c_2\left(\dot{z}_2 - \dot{z}_3\right) + k_2\left(z_2 - z_3\right) - k_1\left(z_1 - z_2\right) - c_1\left(\dot{z}_1 - \dot{z}_2\right) = 0 \\ m_3\ddot{z}_3 + c_3\dot{z}_3 + k_3z_3 - k_2\left(z_2 - z_3\right) - c_2\left(\dot{z}_2 - \dot{z}_3\right) = 0 \\ J_x\ddot{\theta} + d_x\dot{\theta} + \left[\left(k_x + k_y\right)\left(l_1^2 + l_2^2\right) + k_zR_m^2\right]\theta = \left(J_y - J_z\right)\omega\dot{\phi} \\ -me\omega^2\left(l_1 - l_2\right) + \left(F_yl_3 + F_zR_w\right)\cos\Omega - F_xl_3\sin\Omega \\ J_y\ddot{\phi} + d_x\dot{\phi} + \left[\left(k_x + k_y\right)\left(l_1^2 + l_2^2\right) + k_zR_m^2\right]\phi = \left(J_z - J_x\right)\omega\dot{\theta} \\ +me\omega^2\left(l_1 - l_2\right) + \left(F_yl_3 + F_zR_w\right)\sin\Omega + F_xl_3\cos\Omega \end{cases} \tag{8}$$

Among them, m_1, m_2, and m_3 are the masses of the grinding wheel, adapter plate and grinding wheel spindle, k_1, k_2, and k_3 are the stiffness of the joint surface between the three in the Z direction, c_1, c_2, and c_3 are the linear viscous dampers between the three, F_z represents the grinding force of the grinding wheel in the error-sensitive direction during the grinding process, θ, $\varnothing$ respectively indicate the angle of deflection of the rotor around the X axis and Y axis, by consulting the grinding machine design manual, you can obtain the performance parameters related to the grinding machine GP300 as shown in Table 1.

2.2 Dynamic response of the aerostatic spindle system

The second-order Runge-Kutta method is used to solve the dynamic equation of the air spindle system established above. In addition, since the vibration trajectory reflected on the silicon wafer in the actual grinding process is the synthesis of the translational displacement in the delay difference sensitive direction of the spindle system and the swing angle around the X and Y axes, the total synthetic displacement Z_b of each component of the aerostatic spindle system can be expressed as follows:

$$Zb = Z \pm Rw\phi \tag{9}$$

where Z is the displacement of the translational motion in the delay sensitive direction of the spindle system, R_w is the radius of the grinding wheel, and $\varnothing$ is the angle of the spindle swinging around the X and Y axes.

As shown in Fig. 6, the displacement vibration curve of each component after comprehensive consideration of translation and rotation after the solution is solved. It can be seen from the diagram that the motion forms of grinding wheel, adapter plate and spindle rotor are almost the same when considering the participation of grinding force. At the beginning, the movement reaches a larger position, then gradually decreases, and finally tends to be stable. Moreover, the vibration displacement of each component in the Z direction after stabilization shows the law of sinusoidal curve change. From the perspective of the displacement changes after the three are stabilized, the displacement of the grinding wheel changes greatly, the maximum vibration displacement is 0.15 μm, the change of the adapter plate is second, the maximum vibration displacement is 0.13 μm, and the vibration displacement of the spindle rotor changes The smallest, the difference between the highest point and the lowest point is 0.09 μm. In addition, it can be seen from the figure that the grinding wheel spindle system vibrates violently at the beginning, then gradually decreases, and tends to stabilize after 40 s. The reason for this result is that when the grinding wheel is just in contact with the silicon wafer, the axial grinding force of the grinding wheel is the largest, and then the grinding wheel begins to contact the silicon

Table 1 Wafer ultra-precision grinding machine GP300 performance parameters

Spindle system performance parameters	Numeric value
Grinding wheel quality m_1 (kg)	4.75
Adapter plate quality m_2 (kg)	10.24
Spindle rotor quality m_3 (kg)	12
Spindle rotor eccentricity distance e (μm)	2
The distance from the bearing to the center of mass of the rotor (l_1/l_2) (mm)	125/120
The distance from the end of the grinding wheel to the center of mass of the rotor (l_3) (mm)	180
Bonding surface connection stiffness (k_1/k_2) (N/μm)	430
Rotor connection stiffness (k_3) (N/μm)	580
Spindle rotor radius R_m (mm)	70
Grinding wheel radius R_w (mm)	150
The inertia tensor of the spindle rotor around the X and Y axes (J_x/J_y) (gm^2)	5.4
The inertia tensor of the spindle rotor around the Z axis (J_z) (gm^2)	0.19
Angular damping ratio (ε)	0.00005
Linear damping ratio (μ)	0.025

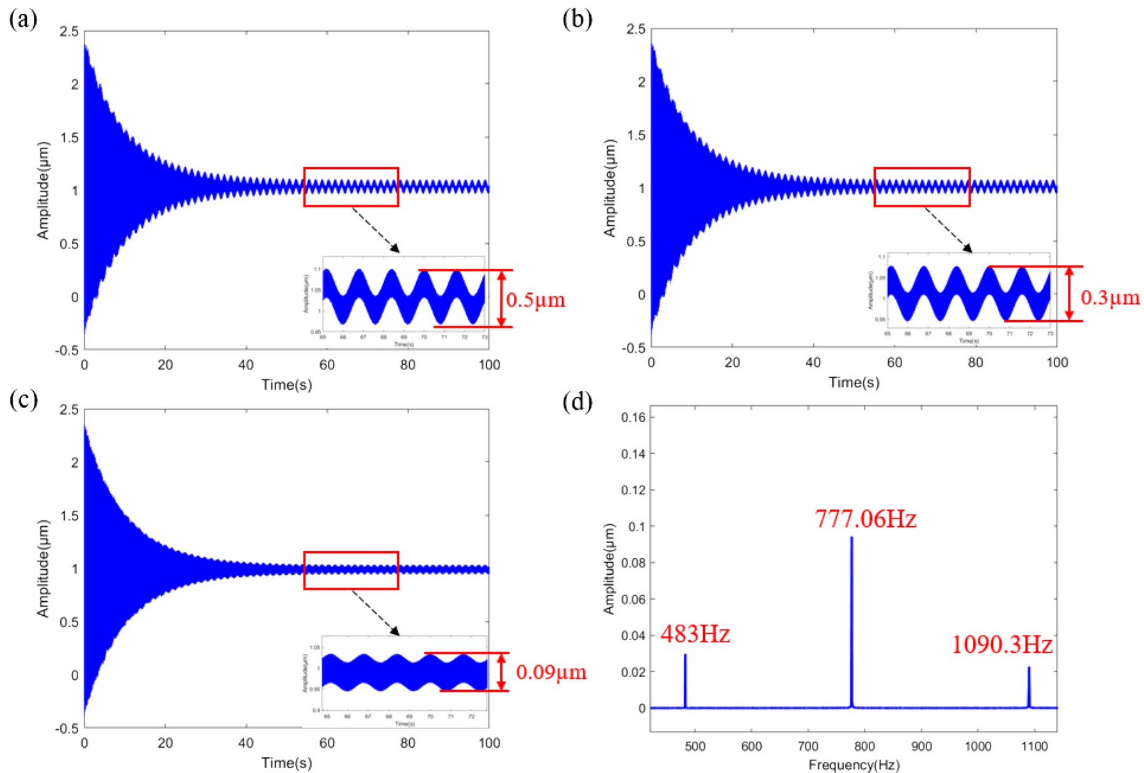

Fig. 6 Aerostatic spindle system dynamics. **a** Grinding wheel synthesis vibration displacement. **b** The adapter plate synthesizes vibration displacement. **c** Spindle rotor synthesizes vibration displacement. **d** Dynamic response frequency of the spindle system

wafer. At this time, the grinding force of the grinding wheel gradually decreases and tends to be stable with the stability of the processing state. By calculating the power spectral density of the displacement vibration curve, the vibration frequencies of the grinding wheel, adapter plate and spindle rotor in the error-sensitive direction during the processing process are analyzed to be 483 Hz, 777.06 Hz, and 1090.3 Hz, respectively.

3 Experiment on vibration response of wafer ultra-precision grinder

For the wafer ultra-precision grinding and polishing machine studied in this paper, in the actual grinding process, the grinding wheel and the end of the workpiece spindle are the weakest links of the whole grinding machine. Therefore, the modal test principle of multi-point excitation and single-point vibration picking is selected in this test. The force hammer is used to knock each measuring point of the grinding machine, and then the sensor is fixed at the position close to the grinding wheel to pick up the vibration signal from each measuring point. Finally, the impact force of the hammer and the vibration response of the grinding wheel end are comprehensively analyzed, and the dynamic amplitude-frequency response of the vibration of the whole machine to the grinding wheel and the workpiece end is obtained

3.1 Whole machine mode test

This modal test uses a high-performance dynamic data acquisition instrument and a corresponding dynamic signal test and analysis system. Before the start of the test, the grinding machine is divided into excitation points in the vibration analysis system software. In this experiment, a total of 309 measuring points are divided for the whole grinding machine. Among them, the point marked with the digital position is taken as the excitation point of the modal test, and the measuring point near the wheel end is taken as the pick point of the modal test. Figure 7 is the division of the measuring points of the whole grinding machine and the selection of the picking points. Since the grinding wheel is fed in the Z direction during grinding, and the Z direction is the error-sensitive direction of the grinding machine. In order to reflect the real processing state, when the force hammer hits the measuring point, the force hammer needs to be struck vertically along the error sensitive direction.

After the hammer strikes each excitation point on the bed in turn, the hammering force of the hammer and the

vibration response of the grinding wheel spindle end are analyzed. The amplitude-frequency response of the vibration of the grinding machine to the spindle end of the grinding wheel is obtained by using the PolyLSCF modal parameter identification method in the dynamic test and analysis system. In addition, in order to ensure the accuracy of the modal test, the modal coherence coefficient after each knock is greater than 0.862, as shown in Fig. 8.

Figure 9 shows the vibration mode test of ultra-precision grinding machine, in which Fig. 9b is the steady-state diagram of the mode test. By finding the steady-state pole marked with s in the diagram, the natural frequencies of each order of the system obtained by the mode test can be calculated. For comparison with the results obtained from the hammer test, the modal analysis software is used to calculate the modal analysis of the grinding machine. After the model material and the applied load are given, the first eight natural frequencies of the delay error sensitive direction (Z direction) in the modal analysis software are compared with the first eight natural frequencies of the hammer test, as shown in Table 2.

It is found that except for the natural frequency error of the 2nd and 6th modes is greater than 6%; the error of the other modal test parameters is less than 6%. In addition, it can be seen from the vibration mode diagram of the whole machine that the vibration effect of the aerostatic spindle and the adapter

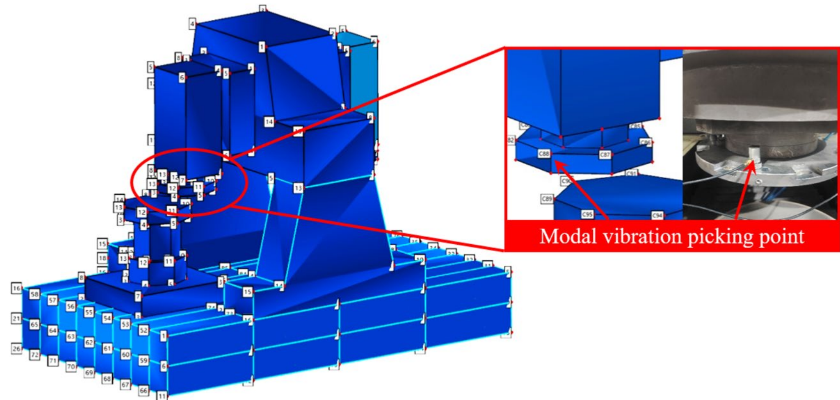

Fig. 7 The whole machine measurement point division and vibration picking point selection

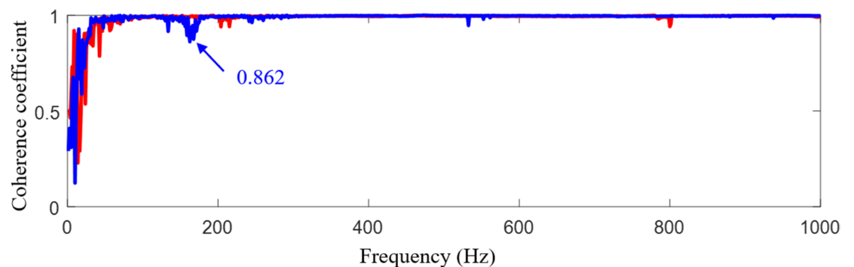

Fig. 8 Coherence function curve of modal test

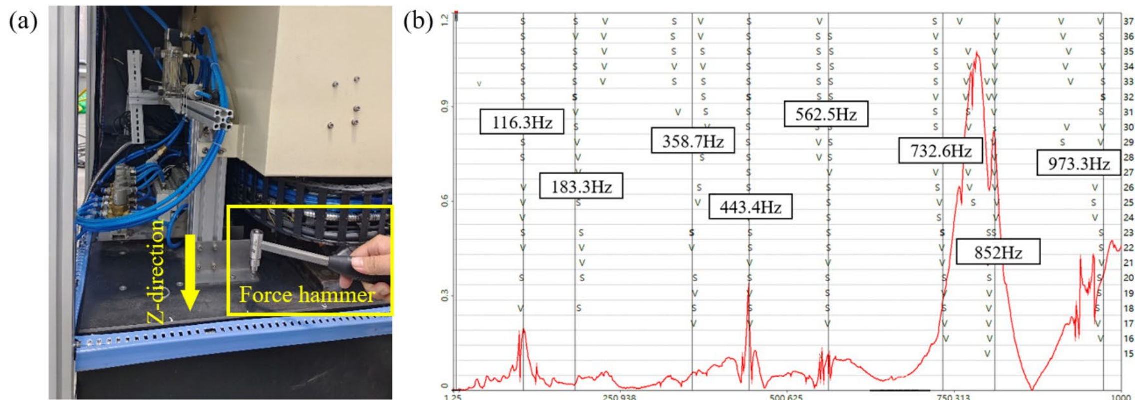

Fig. 9 Wafer ultra-precision grinding machine vibration response experiment. **a** Hammer mode test. **b** Modal test results

Table 2 Comparison of modal experiments and computational pattern recognition parameters

Modal order	Mode shape description	Modal natural frequency		
		Modal testing	Calculate modalities	Error
1	The whole machine is translated up and down	116.3 Hz	121.98 Hz	4.65%
2	The bed and spindle vibrate in the same direction	183.3 Hz	195.35 Hz	6.16%
3	The beam vibrates in reverse	358.7 Hz	368.9 Hz	2.76%
4	The adapter plate vibrates up and down	443.4 Hz	452.17 Hz	1.97%
5	The spindle is torsional from side to side	562.5 Hz	562.23 Hz	0.04%
6	The adapter plate and the spindle are translated in the opposite direction of Z	732.6 Hz	800.69 Hz	8.5%
7	The spindle is translated left and right	852 Hz	899.37 Hz	5.56%
8	The adapter plate is torsional	973.3 Hz	958.41 Hz	4.7%

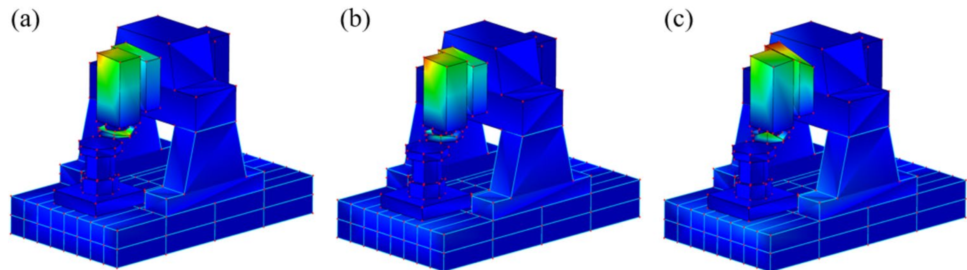

Fig. 10 Modal experimental mode shape. **a** The 4th mode shapes. **b** The 6th mode shapes. **c** The 8th mode shapes

plate is more significant, which is manifested in the 4th, 6th, and 8th modes. Among them, the 4th order is manifested as the up and down vibration of the adapter plate, the 6th order is manifested as the Z-direction reverse translation of the adapter plate and the spindle, and the 8th order is manifested as the torsional vibration of the adapter disk and the grinding wheel spindle feed system. The motion of these vibration modes is in the error sensitive direction during the grinding process, which will cause great error to the silicon wafer after grinding, as shown in Fig. 10.

4 The influence mechanism of aerostatic spindle system dynamics on the waviness error of medium frequency

4.1 Medium frequency waviness feature frequency extraction

In order to extract the characteristic frequency of the intermediate frequency band of the silicon wafer surface after grinding, and to avoid the influence of the change of grinding parameters on the contour frequency of the silicon wafer surface. On the wafer ultra-precision grinding machine with 2000 r/min, 2399 r/min, and 3000 r/min, three different spindle speeds to grind the silicon wafer with a diameter of 300 mm, the silicon wafer grinding test is shown in Fig. 11; the specific grinding parameters are shown in Table 3.

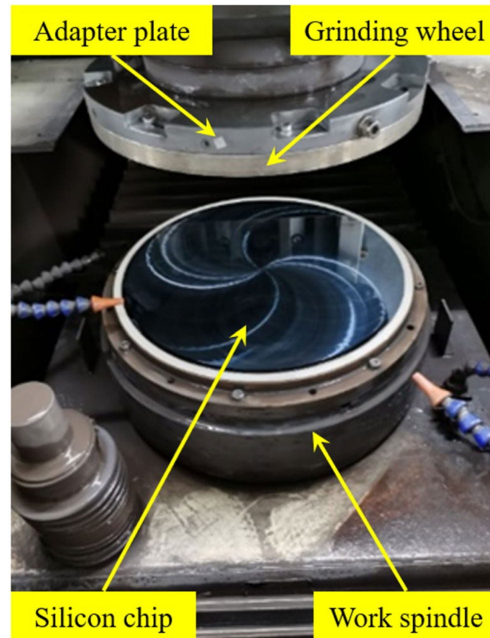

Fig. 11 Wafer grinding test

The vibration acceleration signal in the cutting process is obtained by the acceleration sensor.

The three-dimensional optical surface profiler is used to measure the surface of the silicon wafer after grinding with three grinding parameters, and the frequency band with a

Table 3 Wafer grinding experimental parameters

Grinding parameters	Numeric value
Grinding wheel spindle speed	2000 r/min, 2399 r/min, 3000 r/min
Workpiece spindle speed	110 r/min
Grinding wheel feed speed	5 μm/min
Grinding wheel grinding depth	80 μm

spatial period of 2.5 ~ 33 mm is extracted. The power spectrum calculation is carried out to obtain the spatial frequency components of the surface topography of the three silicon wafers. The spatial frequency of the silicon wafer surface profile has the following corresponding relationship with the time domain vibration frequency [2]:

$$\begin{aligned} \omega &= vf \\ v &= N\pi D/60 \end{aligned} \tag{10}$$

where f represents the spatial frequency of the surface profile curve of the silicon wafer, the unit is 1/mm, v is the tangential speed of the grinding wheel, the unit is mm/s, N is the speed of the grinding wheel spindle, the unit is r/min, D is the diameter of the cup grinding wheel, the unit is mm, ω is the time domain conversion frequency, and the unit is Hz.

The wafer ultra-precision grinding machine uses a cup-shaped diamond grinding wheel with a diameter of 300 mm. According to Eq. (10), the spatial frequency of the silicon wafer surface after three sets of grinding parameters are calculated, as shown in Fig. 12. When the grinding wheel spindle speed is 2000 r/min, there will be three sets of space frequencies of 0.0154 1/mm, 0.0231 1/mm, and 0.0309 1/mm on the silicon wafer grinding surface PSD1; when the grinding wheel spindle speed is 2399 r/min, the silicon wafer grinding surface PSD1 will have three sets of space frequencies of 0.0128 1/mm, 0.0192 1/mm, and 0.0257 1/mm; when the grinding wheel spindle

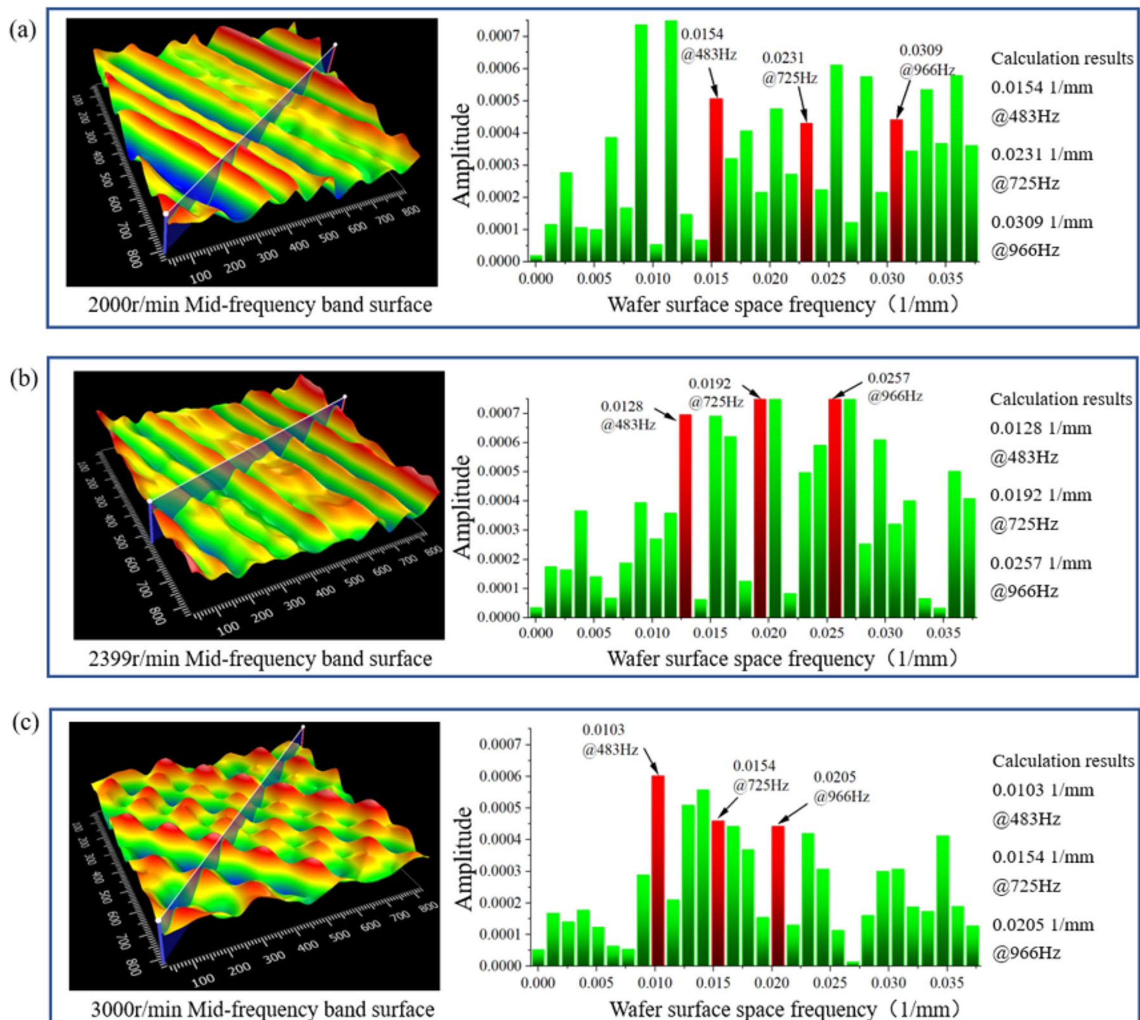

Fig. 12 Frequency distribution of silicon wafer in intermediate frequency band; **a** 2000 r/min silicon wafer surface; **b** 2399 r/min silicon wafer surface; **c** 3000r/min silicon wafer surface

speed is 3000 r/min, the silicon wafer grinding surface PSD1 will have three sets of spatial frequencies: 0.0103 1/mm, 0.0154 1/mm, and 0.0205 1/mm. By converting the spatial frequency into the corresponding time domain frequency by Eq. (10), it can be concluded that when the speed of the grinding wheel spindle increases, the surface space frequency of the silicon wafer decreases after grinding of the three sets of grinding parameters, but the time domain frequency remains unchanged, which is 483 Hz, 725 Hz, and 966 Hz, respectively.

4.2 Medium frequency waviness error traceability analysis

Table 4 compares the characteristic frequencies of the intermediate frequency on the surface of the silicon wafer with the natural frequencies of the 4th, 6th, and 8th order of the mode shape of the grinding wheel spindle system and the characteristic frequencies of the grinding wheel spindle dynamics modeling. From the table, it can be seen that the characteristic frequencies obtained by the dynamic modeling of the grinding wheel spindle system are in good agreement with the experimental results, which proves the correctness of the dynamic model of the aerostatic spindle system. Moreover, the dynamic response frequency of the test and simulation is in good agreement with the intermediate frequency characteristic frequency of the silicon wafer, which proves that the characteristic frequency of the intermediate frequency band of the silicon wafer surface is caused by the dynamic characteristics of the aerostatic spindle system.

In addition, the acceleration signal collected by the accelerometer is calculated by double integration to obtain the vibration displacement curve of the end of the grinding wheel spindle under the actual cutting force. Figure 13 shows the surface topography of the IF band obtained by bandwidth filtering of the ground silicon wafer at this speed. By comparing the surface profile in the grinding direction with the vibration displacement curve of the grinding wheel end, it is found that the peaks of 1, 2, 3, 4, and 5 positions in the frequency band of the silicon wafer are almost the same as the vibration displacement peaks of the grinding wheel end, and the curves of the two are almost consistent. It is proved that the intermediate frequency error of silicon wafer is mainly caused by the dynamic vibration of grinding machine on the surface of silicon wafer.

5 Wafer ultra-precision grinding machine structure improvement

From the results of the second modal experimental mode shape, it can be seen that during the vibration process of the aerostatic spindle system, the vibration deformation of the aerostatic pressure spindle and the grinding wheel adapter plate is more serious. However, since the structure and size parameters of the spindle have been fixed, if you want to reduce the amplitude of the grinding wheel vibration, you can only enhance the stiffness of the adapter by changing the material of the adapter plate or optimizing the structure of the adapter plate, thereby changing the vibration frequency of the aerostatic spindle system, and then reducing the influence of the vibration displacement of the grinding wheel spindle system on the amplitude of the medium frequency ripple error on the silicon wafer processing surface.

In this paper, according to the deformation of the grinding wheel adapter plate during the vibration process of the whole machine, a scheme for optimizing the structure of the adapter plate is given, as shown in Fig. 14. The grinding wheel adapter plate is a uniform disk, the waist-shaped hole on the outer edge is used to fix the grinding wheel, and the internal threaded hole is bolted to the spindle rotor, so two vertically crossed crossbar plates can be added on the upper surface of the adapter plate to enhance the stiffness of the adapter plate, so as to achieve the purpose of reducing the amplitude.

The optimized machine is re-analyzed for modality. Figure 15 shows the modal simulation result of the whole machine after optimization and the displacement vibration curve from the center of the grinding wheel to the edge position of the grinding wheel before and after optimization in the error-sensitive direction of grinding. From the results, it can be seen that the vibration displacement amplitude of the grinding wheel center is larger than the amplitude of the edge, and the displacement amplitude of the center of the grinding wheel after optimization is reduced from 71.68 to

Table 4 Characteristic frequency traceability analysis of medium frequency ripple error on silicon wafer surface

Order	Characteristic frequencies in the mid-frequency band	Grinding machine natural frequency	Spindle dynamic response frequency	Modal shape
4	483 Hz	443.4 Hz	483 Hz	The adapter plate vibrates up and down
6	725 Hz	732.6 Hz	777.06 Hz	Transfer disk and spindle reverse translational
8	966 Hz	973.3 Hz	1090.3 Hz	The adapter plate is torsional

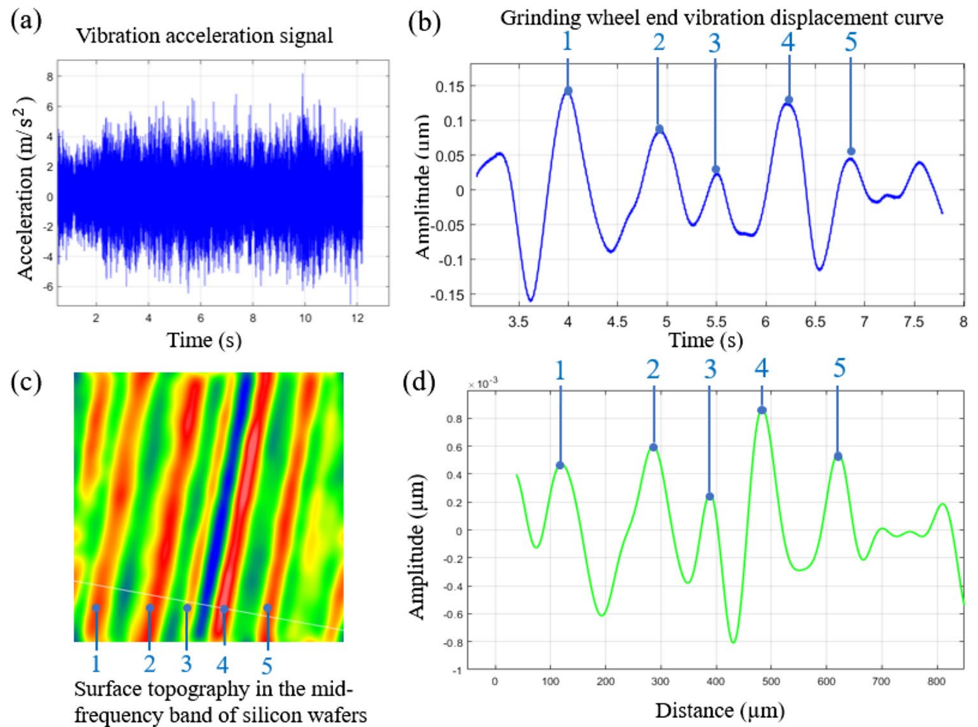

Fig. 13 Grinding wheel vibration displacement curve and silicon wafer medium frequency profile curve extraction. **a** Vibration acceleration signal. **b** Grinding wheel vibration displacement. **c** Surface topography of silicon wafers. **d** Surface profile curve

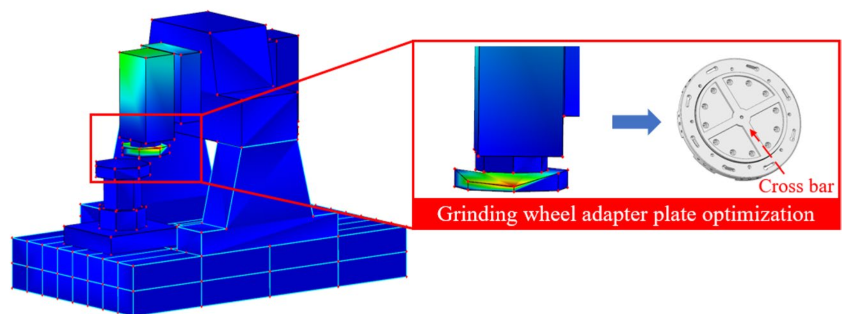

Fig. 14 Optimize the comparison of the structure of the front and rear adapter plate

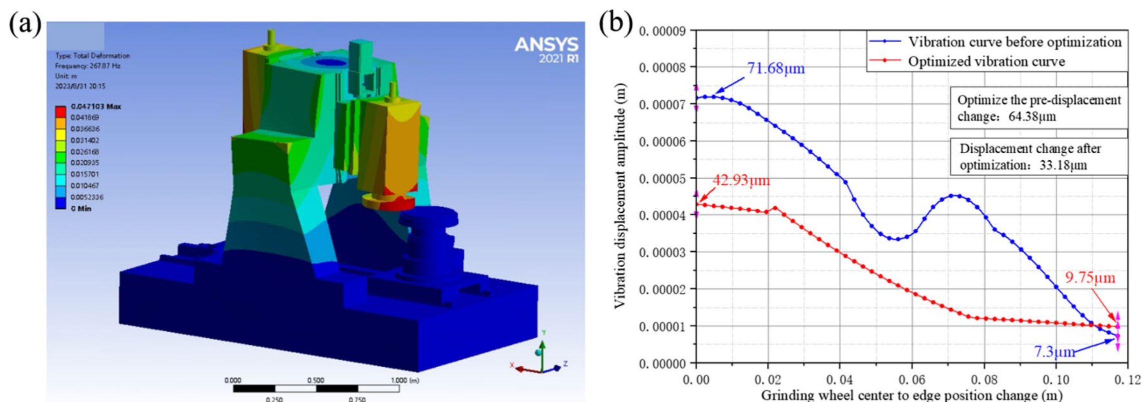

Fig. 15 Grinding machine calculation modal analysis. **a** Modal mode shape results. **b** Optimize the comparison of vibration displacement at the end of the grinding wheel before and after

42.93 μm, and the maximum displacement change of the grinding wheel from the center to the edge Z direction before optimization is 64.38 μm, and the displacement change after optimization is 33.18 μm, which is 52.8% lower than that before optimization. It shows that changing the structure of the adapter plate can reduce the vibration displacement at the end of the grinding wheel spindle, and the optimization effect is remarkable.

6 Conclusions

This paper reveals the influence of the dynamic characteristics of wafer ultra-precision grinding machine on the medium frequency waviness error of silicon wafer surface from three aspects: modal test, theoretical modeling and simulation analysis, and the specific conclusions are as follows:

1) The vibration displacement curve of the delay difference sensitive direction of the aerostatic pressure spindle system was obtained by theoretical modeling and modal test, and the vibration response frequencies of the spindle system were obtained by power spectrum analysis, which were 483 Hz, 777.06 Hz, and 1090.3 Hz, respectively.
2) The characteristic frequencies of the intermediate frequency band on the surface of the silicon wafer during processing were extracted, and it was found that the characteristic frequency of the intermediate frequency on the surface of the silicon wafer was consistent with the frequency of the dynamic response of the grinding machine. The vibration curve of the end of the grinding wheel spindle during the grinding process is compared with the intermediate frequency contour curve of the silicon wafer surface. The two curves are almost consistent, which proves that the intermediate frequency ripple on the silicon wafer surface is caused by the dynamic characteristics of the grinding machine.
3) A scheme for improving the structure of the adapter plate was proposed, and the amplitude change of vibration displacement at the end of the grinding wheel after the improvement was reduced by 52.8% compared with the previous one, indicating that the improved scheme was effective.

Author contributions RK contributed significantly to analysis and manuscript preparation;

XZ contributed to the conception of the study;

JL performed the experiment;

ML performed the data analyses and wrote the manuscript;

JX helped perform the analysis with constructive discussions;

Funding This research is financially supported by the Program of National Natural Science Foundation of China (51991372), The Opening Foundation of Key Laboratory for Precision and Non-traditional Machining Technology (No. B202102) and The Key Support Plan for Foreign Experts (No. ZCZD2022002L).

Data availability Data used to support the findings of this study are available from the corresponding author upon request.

Code availability Not applicable.

Declarations

Ethics approval Not applicable.

Consent to participate Not applicable.

Consent for publication Not applicable.

Competing interests The authors declare no competing interests.

References

1. Gao S, Huang H, Zhu XL, Kang RK (2017) Surface integrity and removal mechanism of silicon wafers in chemo-mechanical grinding using a newly developed soft abrasive grinding wheel. Mater Sci Semicond Process 63:97–106. https://doi.org/10.1016/j.mssp.2017.02.001
2. Li JS, Wei W, Huang X, Liu PK (2020) Study on dynamic characteristics of ultraprecision machining and its effect on medium-frequency waviness error. Int J Adv Manuf Technol 108:2895–2906. https://doi.org/10.1007/s00170-020-05557-7
3. Tao HF, Liu YH, Zhao DW, Lu XC (2022) Effects of wheel spindle vibration on surface formation in wafer self-rotational grinding process. Int J Mech Sci 232. https://doi.org/10.1016/j.ijmecsci.2022.107620
4. Yang X, An CH, Wang ZZ, Wang QJ, Peng YF, Wang J (2016) Research on surface topography in ultra-precision flycutting based on the dynamic performance of machine tool spindle. Int J Adv Manuf Technol 87:1957–1965. https://doi.org/10.1007/s00170-016-8583-7
5. Guo MX, Jiang XH, Ding ZS, Wu ZP (2018) A frequency domain dynamic response approach to optimize the dynamic performance of grinding machine spindles. Int J Adv Manuf Technol 98:2737–2745. https://doi.org/10.1007/s00170-018-2444-5
6. Wu QH, Sun YZ, Chen WQ, Chen GD (2017) Theoretical and experimental investigation of spindle axial drift and its effect on surface topography in ultra-precision diamond turning. Int J Mach Tools Manuf 116:107–113. https://doi.org/10.1016/j.ijmachtools.2017.01.006
7. Gao Q, Zhao H, Lu LH, Chen WQ, Zhang FH (2020) Investigation on the formation mechanism and controlling method of machined surface topography of ultra-precision flycutting machining. Int J Adv Manuf Technol 106:3311–3320. https://doi.org/10.1007/s00170-019-04869-7
8. Chen DJ, Li SP, Zhang X, Fan JW (2022) Relationship between dynamic characteristics of air film of aerostatic spindle and mid-frequency of surface topography. Adv Manuf 10:428–442. https://doi.org/10.1007/s40436-022-00391-4
9. Dong ZW, Zhang SJ, Xiong ZW, Rao XX (2018) A generalized dynamic model for spindle vibration influencing surface topography in different ultra-precision machining processes. Int

J Adv Manuf Technol 96:2471–2478. https://doi.org/10.1007/s00170-018-1814-3
10. Chen JB, Fang QH, Li P (2015) Effect of grinding wheel spindle vibration on surface roughness and subsurface damage in brittle material grinding. Int J Adv Manuf Technol 91:12–23. https://doi.org/10.1016/j.ijmachtools.2015.01.003
11. Liu L, Lu LH, Gao Q, Zhang R, Chen WQ (2017) External aerodynamic force on an ultra-precision diamond fly-cutting machine tool for kdp crystal machining. Int J Adv Manuf Technol 93:4169–4178. https://doi.org/10.1007/s00170-017-0850-8
12. Meng QY, Guo B, Wu GC, Xiang Y, Guo ZF, Jia JF, Zhao QL, Li KN, Zeng ZQ (2023) Dynamic force modeling and mechanics analysis of precision grinding with microstructured wheels. J Mater Process Technol 314. https://doi.org/10.1016/j.jmatprotec.2023.117900
13. Yin L, Liu QX, Zhang F, Zhou ZR, Ullah S (2019) Study for the identification of dominant frequencies and sensitive structure on machine tools using modal decoupling and structural sensitivity analysis. J Vib Eng Technol 7:507–517. https://doi.org/10.1007/s42417-019-00172-7
14. Niu J, Ding Y, Geng ZM, Zhu LM, Ding H (2018) Patterns of regenerative milling chatter under joint influences of cutting parameters, tool geometries, and runout. J Manuf Sci Eng J MANUF SCI E-T ASME 140. https://doi.org/10.1115/1.4041250
15. Wei RC, An CH, Wang ZZ, Xu Q, Lei XY, Zhang JF (2020) Dynamic performance analysis and quantitative evaluation for ultraprecision aerostatic spindle. Proc Inst Mech Eng B: J Eng Manuf 234:218–228. https://doi.org/10.1177/0954405419855239
16. An CH, Deng CY, Miao JG, Yu DP (2018) Investigation on the generation of the waviness errors along feed-direction on flycutting surfaces. Int J Adv Manuf Technol 96:1457–1465. https://doi.org/10.1007/s00170-018-1720-8
17. Ding YY, Rui XT, Chang Y, Lu HJ, Chen YH, Ding JG, Shehzad A, Chen GL, Gu JJ (2023) Optimal design of the dynamic performance of the ultra-precision fly cutting machine tool. Int J Adv Manuf Technol 124:567–585. https://doi.org/10.1007/s00170-022-10502-x
18. Yao WH, Kang RK, Guo XG, Zhu XL (2022) Effect of grinding residual height on the surface shape of ground wafer. J Mater Process Technol 299. https://doi.org/10.1016/j.jmatprotec.2021.117390
19. Chen D, Li S, Fan J (2022) A 3d turning surface model under the action of coupling dynamics of aerostatic spindle and cutting system. Int J Adv Manuf Technol 120:4617–4633. https://doi.org/10.1007/s00170-022-09006-5
20. Tao HF, Liu YH, Zhao DW, Lu XC (2022) The material removal and surface generation mechanism in ultra-precision grinding of silicon wafers. Int J Mech Sci 222. https://doi.org/10.1016/j.ijmecsci.2022.107240
21. Sun C, Niu YJ, Liu ZX, Wang YS, Xiu SC (2017) Study on the surface topography considering grinding chatter based on dynamics and reliability. Int J Adv Manuf Technol 92:3273–3286. https://doi.org/10.1007/s00170-017-0385-z
22. Zhu YD, Zhang QL, Zhao QL, To S (2021) The material removal and the nanometric surface characteristics formation mechanism of tic/ni cermet in ultra-precision grinding. Int J Refract Met Hard Mater 96. https://doi.org/10.1016/j.ijrmhm.2021.105494
23. Li D, Qiao Z, Walton K, Liu YT, Xue JD, Wang B, Jiang XQ (2018) Theoretical and experimental investigation of surface topography generation in slow tool servo ultra-precision machining of freeform surfaces. Materials (Basel) 11. https://doi.org/10.3390/ma11122566
24. Yin TF, Du HH, Zhang GQ, Hang W, To S (2023) Theoretical and experimental investigation into the formation mechanism of surface waviness in ultra-precision grinding. Tribol Int 180. https://doi.org/10.1016/j.triboint.2023.108269
25. Zhang CD, Yu WN, Yin L, Zeng Q, Chen ZX, Shao YM (2023) Modeling of normal contact stiffness for surface with machining textures and analysis of its influencing factors. Int J Solids Struct 262-263. https://doi.org/10.1016/j.ijsolstr.2022.112042
26. Zhu XL, Li Y, Dong ZG, Kang RK, Gao S (2020) Study into grinding force in back grinding of wafer with outer rim. Adv Manuf 8:361–368. https://doi.org/10.1007/s40436-020-00316-z
27. Zhang SJ, To S, Cheung CF, Wang HT (2012) Dynamic characteristics of an aerostatic bearing spindle and its influence on surface topography in ultra-precision diamond turning. Int J Mach Tools Manuf 62:1–12. https://doi.org/10.1016/j.ijmachtools.2012.04.007

Publisher's Note Springer Nature remains neutral with regard to jurisdictional claims in published maps and institutional affiliations.

Springer Nature or its licensor (e.g. a society or other partner) holds exclusive rights to this article under a publishing agreement with the author(s) or other rightsholder(s); author self-archiving of the accepted manuscript version of this article is solely governed by the terms of such publishing agreement and applicable law.